



An Accurate Aneurysm Detection Model based on Artificial Intelligence

Meltem YAVUZ ÇELİKDEMİR¹, Ayhan AKBAL²

¹ Tatvan Vocational School, Bitlis Eren University, Bitlis, Türkiye

² Department of Electrical and Electronics Engineering, Fırat University, Elazığ, Türkiye

✉: mycelikdemir@beu.edu.tr  [0000-0003-0552-2601](https://orcid.org/0000-0003-0552-2601)  [0000-0001-5385-9781](https://orcid.org/0000-0001-5385-9781)

Geliş (Received): 29.04.2025

Düzeltilme (Revision): 11.06.2025

Kabul (Accepted): 30.06.2025

ABSTRACT

Cerebral aneurysms are a major, life threatening cerebrovascular disease, and accurate interpretation of Computed Tomography Angiography (CTA) is critical for early diagnosis and treatment. This study evaluates the effectiveness of deep learning in reducing radiologist related interpretation errors by applying 15 different Convolutional Neural Networks (CNNs) to 1,211 CTA images. Prior to classification, images underwent various preprocessing and filtering operations, and comparative performance metrics were obtained. The best result, representing the highest accuracy reported to date of 99.72%, was achieved with a smoothing filtered image dataset using the VGG19 architecture. In the VGG19 test set, model outputs consisted of 272 true negatives (tn), 1 false negative (fn), 0 false positives (fp), and 90 true positives (tp). These findings demonstrate that appropriate image preprocessing and filtering significantly enhance CNN based aneurysm detection performance and play a crucial role in improving classification accuracy.

Keywords: Artificial Intelligence, Cerebral Aneurysm, Image Filtering, CTA Scan

Yapay Zeka Tabanlı Doğru Bir Anevrizma Tespit Modeli

ÖZ

Serebral anevrizmalar, yaşamı tehdit eden önemli serebrovasküler hastalıklardır ve erken tanı ve tedavi için Bilgisayarlı Tomografi Anjiyografisi'nin (BTA) doğru yorumlanması kritik öneme sahiptir. Bu çalışma, 1211 BTA görüntüsüne 15 farklı Evrişimli Sinir Ağı (ESA) uygulanarak, derin öğrenmenin radyolog kaynaklı yorumlama hatalarını azaltmadaki etkinliğini değerlendirmektedir. Sınıflandırma öncesinde görüntülere çeşitli ön işleme ve filtreleme işlemleri uygulanmış ve karşılaştırmalı performans metrikleri elde edilmiştir. En iyi sonuç, literatürde şimdiye kadar bildirilen en yüksek doğruluk oranı olan %99,72 ile yumuşatma filtresi uygulanmış görüntü veri setinde VGG19 mimarisi kullanılarak elde edilmiştir. VGG19 test setinde model çıktıları 272 gerçek negatif (tn), 1 yanlış negatif (fn), 0 yanlış pozitif (fp) ve 90 gerçek pozitiften (tp) oluşmuştur. Bu bulgular, uygun görüntü ön işleme ve filtreleme adımlarının, CNN tabanlı anevrizma tespit performansını anlamlı ölçüde artırdığını ve sınıflandırma doğruluğunu iyileştirmede kritik bir rol oynadığını göstermektedir.

Anahtar Kelimeler: Beyin Anevrizması, BTA Tarama, Görüntü Filtreleme, Yapay Zeka

INTRODUCTION

In parallel with an ever increasing global population, with each passing day health problems are also on the rise. Among the major health issues is the formation of cerebral aneurysms [1], defined as protruding enlargements of cerebral arteries [2]. The main risk for patients with a cerebral aneurysm is the rupture of the aneurysm and the resulting fatal brain hemorrhage. Therefore, early detection of cerebral aneurysms prior to their rupture is of vital importance. Although unruptured aneurysms have been detected in 3% of the human population, new research has shown that this rate may actually be as high as 11% [1]. This life threatening condition is frequently addressed by researchers in the fields of medicine and engineering [3]. As technology

has developed, advances have occurred in aneurysm diagnosis methods and techniques. These diagnostic methods include Computed Tomography Angiography (CTA), Digital Subtraction Angiography (DSA), and Magnetic Resonance Angiography (MRA). Angiography images enable increased diagnosis of unruptured aneurysms with high accuracy. In this context, the use of cerebral CTA images represents an important step in the detection and early treatment of cerebral aneurysms. The processing steps implemented in digital environments are expected to produce more accurate results with respect to diagnosis and determining the appropriate treatment method.

Aneurysms are detected in CTA, MRA, and DSA images whose deep features are derived from Deep learning (DL)

based studies in this field [4]. In order to classify the disease with high accuracy, it is envisaged that CTA images will be preprocessed and used in deep neural networks. In this study, a DL based approach, founded on the detection of aneurysm disease in CTA images, was implemented. Image classification with and without aneurysms was performed in 15 different Convolutional Neural Networks (CNN), which are DL architectures. CTA images of 230 patients who had sought treatment in the neurosurgery outpatient clinic of Firat University Hospital within the last 10 years were examined. In addition to the brain CTA raw images obtained from 200 patients with and 30 patients without aneurysms, the images to which the necessary preprocessing and filtering methods were applied were used as input information in CNNs. After the training process was completed in CNNs, the CTA images obtained from the patients were classified as either aneurysm or healthy brain. Using this method, the presence of aneurysms was detected with the highest accuracy reported to date, thereby contributing to the literature.

Manual scanning of aneurysms in CTA images necessitates systems that can provide more rapid and precise outcomes [5]. Responding to this need, rapid advancements in technology have increased the prevalence of AI and DL based methods aimed at automating cerebral aneurysm detection [6,7]. There is significant potential to improve the accuracy of AI based detection of intracranial aneurysms using CTA. In this regard, 212 patients who underwent CTA and DSA were included in a study evaluating three different methods for aneurysm detection: artificial intelligence, doctors, and artificial intelligence doctors. Aneurysms were diagnosed using DSA for 179 of the patients, with a total of 224 aneurysms analyzed. The resulting performance metrics calculated for the use of artificial intelligence in the diagnosis of aneurysms were 74.5% accuracy, 84.9% sensitivity, and 18.2% specificity [8].

Various DL models have been developed for intracranial aneurysm detection. However, the performance of these models based on aneurysm detection has yet to be evaluated. The impact of the models has been measured using meta analysis, taking into consideration performance evaluation and the assistance that they would provide to clinicians. Aneurysm detection has been reported as having a patient level sensitivity of 92%, a specificity of 96%, and a lesion level sensitivity of 92% [5]. DSA images have been used in a DL algorithm developed for the automatic detection of intracranial aneurysms. A total of 75 cases in the training set, along with 20 and 35 cases in the internal and external test sets, respectively, were evaluated based on a three dimensional U-Net. Within the scope of the study, a five fold cross validation was performed. The sensitivity rates obtained were 94.4% for the training and internal test sets and 82.9% for the external test set. Aneurysms were detected with an accuracy rate of 81.8% for women and 84.6% for men [9].

In a study aimed at DL based detection of stroke, a neurological disease caused by the occlusion of a cerebral

vessel, Magnetic Resonance Imaging (MRI) images in the dataset were preprocessed, while deep features were extracted using pretrained CNNs Resnet101 and DenseNet201. The accuracy of the model presented in the study was evaluated using three different datasets; the calculated results were 97.56%, 99.32%, and 99.16% [10]. Artificial intelligence based software designed to detect aneurysms in TOF-MRA (Time Of Flight-MRA) was evaluated, with 191 images in the dataset analyzed using “mdbrain” software. While the expert reader detected 54 aneurysms, the sensitivity of the software was calculated as 72.6%, with a specificity of 87.2% and 82.6% accuracy. The positive predictive value was found to be 67.9% and the negative predictive value was 88.5%. It resulted in a low detection rate of 33.3% and 16.7% for fusiform and thrombosed aneurysms, respectively; however, for saccular aneurysms exceeding 5 mm, the sensitivity was 100% [11]. In another study, 1177 digital bone subtraction CTA scan images were trained with a DL based model to automatically detect intracranial aneurysms. The classification accuracy of the model, which was designed to reduce the workload of radiologists, was 99% [12]. TOF-MRA images of cerebral aneurysms from three different institutions obtained between 2006 and 2019 were evaluated in another study, in which internal testing used images for 80% training and 20% testing. Exclusion criteria were aneurysms greater than 15 mm and images without aneurysms. Three different DL models, 2D-CNN, 3D-CNN, and MD-CNN, were trained for voxel based aneurysm detection. A total of 732 aneurysms in the 559 cases were included in the study. The highest sensitivities were found to be 80.4%, 87.4%, and 82.5%, respectively, with 6.1, 7.1, and 5.0 false positives per case. In the external testing process, the sensitivities were 82.1%, 86.5%, and 89.1%, while false positives per case were 5.9, 7.4, and 4.2 [13].

A novel method has also been proposed for aneurysm detection. In the first stage, the cerebral artery segmentation algorithm was used to determine the relevant region. A 3D U-Net model was developed by 3D SEnet module to detect aneurysms. The dataset consisted of 231 MRA images to be applied in 132 training sets, 34 internal and 65 external test sets. The sensitivity of this method was calculated at 97.89% with five fold cross validation and 90.8% with a false positive rate per case of 2.47 in the external test set [14]. Another study aimed to develop a computer aided aneurysm detection method to improve the diagnostic accuracy of cerebral aneurysms while reducing the rate of false positives. A total of 1160 TOF-MRA datasets, 1096 with aneurysms and 166 without, were divided into 1037 training sets and 123 test sets. The detection model based on dual channel SE-3D UNet was trained with five fold cross validation. This method achieved a sensitivity of 82.46% at the patient level and 73.85% at the lesion level, with 0.88 false positives per case [15].

A dataset consisting of 500 images in the training set and 86 images in the test set was trained and tested using CNN. Accuracy was calculated at 98.8% with an AUC of

0.87 [16]. Training was carried out with CNN for 214 patients, of whom 83 had cerebral aneurysms and 131 were healthy control subjects. The model performed at 95% accuracy with an AUROC of 0.95 [17]. Disease was diagnosed by applying CNN models incorporating 1112 acute ischemic infarction images and 1202 normal diffusion MR images. Greater than 90% classification accuracy was achieved using pretrained AlexNet, ResNet101, ResNet50, DenseNet201, and DarkNet19 models [18]. A total of 450 MRA scan images with intracranial aneurysms were used with CNN, of which 300 were reserved for training, 50 for parameter settings, and 100 for final evaluation. Aneurysm detection was calculated at 94.2%, with 70% sensitivity and 2.9 false

positives per case [19]. In another study comprised of 51 patients with CTA, 57 out of 60 aneurysms were detected by means of an artificial intelligence software program. Sensitivity, specificity, and positive and negative predictive values were 95%, 100%, 100%, and 99.7%, respectively. In addition, an accuracy rate of 99.7% in detecting cerebral aneurysms was obtained [20]. One study demonstrated the usefulness of convolutional neural networks in identifying brain areas involved in the progression of cognitive impairment by employing standard magnetic resonance imaging (MRI) sequences [21].

Table 1. Literature studies on automatic cerebral aneurysm detection

Ref.	Diagnosis	Accuracy (%)	Sensitivity (%)	Specificity (%)	Method	Patient	Aneurysm
[8]	DSA	74.5	84.9	18.2	DL	179	224
[5]	N/A	N/A	92	96	DL	N/A	N/A
[9]	DSA	N/A	94.4	N/A	U-Net	130	N/A
[25]	CTA	99	N/A	N/A	DL	1177	N/A
[11]	MRA	82.6	72.6	87.2	DL	N/A	191
[13]	MRA	N/A	89.1	N/A	CNN	559	732
[14]	MRA	N/A	97.89	N/A	U-Net	231	N/A
[26]	MRA	N/A	86.2	N/A	DL	200	411
[27]	DSA	84.5	89	N/A	RetinaNet	275	250
[15]	MRA	N/A	82.46 (patient) 73.85 (lesion)	N/A	U-Net	1160	1096
[17]	N/A	95	N/A	N/A	CNN	214	81
[16]	N/A	98.8	N/A	N/A	CNN	586	N/A
[28]	MRA	N/A	N/A	N/A	AlexNet	N/A	N/A
[19]	MRA	94.2	70	N/A	CNN	450	N/A
[29]	MRA	97.19	95.87	100	U-Net	40	N/A
	DSA	90.2	91.46	86.01			
[20]	CTA	99.7	95	100	DL	51	60
[30]	DSA	93.5	N/A	N/A	CNN	261	N/A
[31]	TCD	N/A	86	86	VGG16	278	N/A
[32]	CT	N/A	91.8	N/A	R-CNN	311	352
			For >3mm 96.7				
[33]	MRA	N/A	93	N/A	ResNet18	683	748
				N/A	VGG16, ResNet50, InceptionResNetV2, InceptionV3, DenseNet121, EfficientNetB6		
[34]	CT	95.99 EfficientNetB6	N/A		AlexNet, VGG16, VGG19, ResNet18, ResNet50, ResNet101, GoogLeNet, InceptionResNetV2, InceptionV3, MobileNetV2, NASNetMobile, DenseNet201, ShuffleNet, SqueezeNet, Xception	N/A	2500
Our	CTA	99.72 VGG19 (Smoothing)	99.63	100		246	1211

Research aimed at removing noise components by applying filter types to MR images evaluated the utility of these filters using PSNR (Peak Signal to Noisy Rate) and SSIM (Structural Similarity Index) performance metrics. The applied filters were not observed to have a dominant algorithm yielding the best results for all images, nor was there a clear difference with respect to PSNR and SSIM scores [22]. A CNN based image segmentation method, in which Gaussian and Laplace filters were applied to CTA images, was evaluated for cerebral aneurysms. Multi modal CNN training was performed utilizing both the original and processed images. The performance of the segmentation effect was found to be at the maximum level when the threshold value was 0.95 [23]. In another study, three dimensional T1 weighted magnetic resonance images were preprocessed using axis transformation, image reorientation, normalization, modulation, segmentation, noise removal, and smoothing steps [24].

Table 1 provides an overview of recent literature on cerebral aneurysm detection, demonstrating that DL models have been widely adopted for this purpose using data from various imaging modalities, including CTA, MRA, DSA, and CT. The performance metrics reported in these studies particularly classification accuracy, sensitivity, and specificity are generally high, reflecting the effectiveness of DL based approaches in this domain. As a result, recent research has increasingly focused on developing and refining such models to further improve diagnostic performance. However, the variability in results across studies highlights the ongoing need for even more accurate and robust detection methods. In response to this need, our study introduces an image filtering architecture designed to enhance input data quality and maximize the performance of DL models in cerebral aneurysm detection. This approach aims to address existing limitations in the literature and contribute to the advancement of automated diagnostic systems.

Motivation

Existing research in the literature predominantly utilizes preexisting datasets [35–38]. While DL studies relying on these datasets yielded a high accuracy rate, accuracy rates decreased when real datasets were utilized. Researchers have proposed a DL algorithm for aneurysm detection that uses a preexisting TOF-MRA dataset [38]. Aneurysm detection has also been carried out by analyzing DSA images from a ready dataset provided by the Cerebral Aneurysm Detection and Analysis (CADA) competition [35]. Other studies in the literature have explored similar topics [37,39–42].

Existing literature on DL for cerebral aneurysm detection often relies on preexisting datasets and lacks comprehensive exploration of image filtering techniques. While high accuracy rates have been reported, performance often decreases when these models are applied to real world datasets. To address these gaps, the objective of the present study is to attain the highest known value of accuracy in the automatic detection of

cerebral aneurysms by introducing a novel dataset that is not available in the literature and is used for the first time. An additional motivation for this study is to utilize image filtering methods that have not previously been applied to CTA images in the literature as input information to CNNs. By leveraging these image filtering techniques, specifically applied to CTA images, as input to CNNs, our approach aims to achieve state of the art accuracy in automatic aneurysm detection, enhancing classification performance through optimized image preprocessing. This strategy has resulted in increased training accuracy during classification and demonstrates the potential of combining novel datasets with advanced image processing methods to bridge existing gaps in the field. This study primarily aims to develop a DL approach for the automatic identification of brain aneurysms using CTA images of the brain. The research employing this DL method was conducted in four distinct phases. Initially, a dataset comprising images of healthy individuals without aneurysms and patients with aneurysms of varying sizes and locations was generated from CTA scans obtained from participants. In the second stage, these images were processed using five different filtering techniques. Next, the images were applied as input into 15 different CNNs to detect aneurysms in the filtered images; for this purpose the CTA images were then classified. In the final stage, the performance of the system was analyzed, and the accuracy, precision, specificity, sensitivity, and F-score parameter values were calculated.

Main contributions and novelties

The contributions of this study are listed below.

- Medical image usage is common in high accuracy classification applications for DL models. In this study, we propose filters as an alternative approach for high performance in DL models.
- The proposed method integrates image filtering with CNNs to generate combined feature representations, resulting in the highest observed classification accuracy of 99.72%.

The novelties of this study are listed below.

- This study achieves state of the art performance in disease detection by integrating advanced image enhancement techniques with deep feature extraction, outperforming conventional DL architectures.
- For this, we used preprocessing steps in the image in addition to the deep feature extractions applied in learning.
- We improved the clarity of disease symptoms more apparent with CTA image denoising, image smoothing, and sharpening filters.

The new datasets created were used in CNNs.

DATASET

The dataset utilized in this study consists of non contrast brain CT images obtained from patients who presented to the Neurosurgery Outpatient Clinic of Firat University Hospital. CT images from 230 patients with suspected

brain aneurysms were extracted from the hospital's PACS database. Of these, 200 patients were diagnosed with an aneurysm, while 30 individuals were confirmed as healthy controls. The diagnostic process involved a detailed review of radiology reports prepared by radiology specialists, and all cases were further verified by three experienced neurosurgeons to ensure the accuracy of the labels. The brain CT images comprise a series of coronal sections acquired at 0.5 mm intervals, providing high resolution visualization for the detection of aneurysms. Each patient's CT scan was stored as a video file, with the number of images per video ranging from 600 to 1200 frames. The original images were formatted in the ".dicom" extension, which requires substantial memory resources. For data preprocessing, the DICOM images were imported into MATLAB, and the videos were manually divided into individual frames using the DICOM browser application. To reduce computational load and enhance usability during model training and testing, 20–30 representative images were selected for each patient and converted to JPEG format. In total, 1,211 images were included in the dataset, comprising 911 images from aneurysm positive cases and 300 from healthy controls. Images depicting aneurysms from various angles were specifically chosen according to the requirements of image processing and as input for the CNN model.

PROPOSED FILTERING METHODS

Brain CTA images of healthy and diseased patients were preprocessed prior to their use in CNN. In the first stage,

the images were formatted with the extension ".dicom" before being converted to ".jpg" when the dataset was created. Next, all CTA images formatted with .jpg extensions of varying pixel resolutions were resized to 512x512 pixel resolution. The resulting images underwent filtering after the necessary image preprocessing steps were completed. During the filtering process, matrices consisting of 3x3 and 8x8 structures were scanned onto the images. For overlapping values, the multiplication results were added together and the final values were obtained by dividing by the sum of the filter elements [43]. Since there was no color loss in the brain CTA grayscale images used, more accurate results were obtained with the filters applied during the image processing step. Median and smoothing filters, which are frequently encountered in the literature, were applied to brain CTA images to reduce noise and provide smoothing, while Sobel, Canny, and Prewitt filters were used for edge detection. These procedures aimed to increase the success rate in disease detection by providing clearer images to CNN models. A total of 15 different CNN models were trained for both the original brain CTA images and those enhanced using various filtering techniques and image preprocessing filters. The effect of these models on the results was subsequently examined. The image processing principle diagram, showing the use of CNN following the filtering and preprocessing steps applied to the original images, is presented in Figure 1.

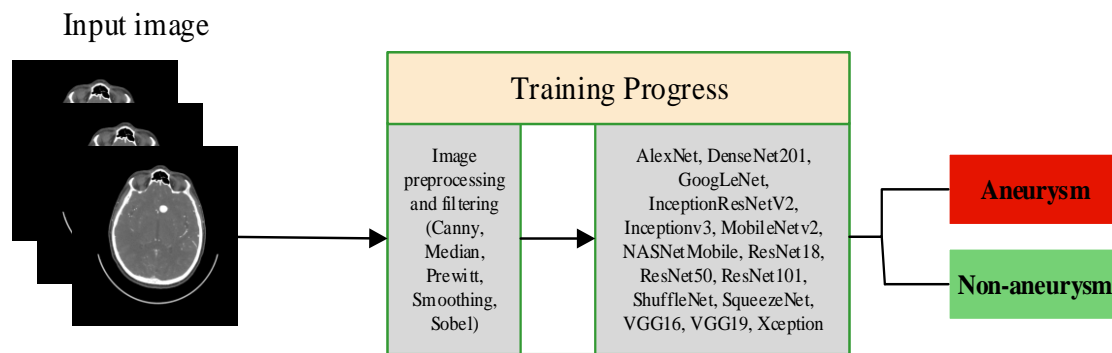


Figure 1. Classification of filtered CTA images

Clearer images were obtained by applying five different filtering techniques for noise removal, smoothing, and edge detection through image preprocessing steps. The filtering methods employed were the Canny, median, Prewitt, Sobel, and smoothing filters.

The Canny edge detection algorithm was applied to the brain CTA images obtained in the dataset. The primary factor in utilizing this algorithm is that the effective detection ability per edge yields good results. In the first stage, noise is eliminated; next, intensity gradients are located and gradient magnitude thresholding is applied, identifying potential edges. In the final stage, edge detection is verified by reducing weak and disconnected edges. Due to its gradual structure, the error rate in this algorithm is low [44]. The Canny filter is superior at

detecting weak edges and is less likely to be misled by noise compared to other filters.

Median filtering method is used to reduce the noise rate present in images and prevent loss of detail. When performing median filtering, neighboring pixel values are arranged respectively in the desired region of 3x3 and 8x8 matrix size on the image data, and the median pixel value is taken as the basis. Choosing the median value reduces deviation by eliminating the presence of extreme values, thus eliminating noise in the newly obtained image. Noise removal, the preprocessing step for retinal fundus image classification, has been performed using median filtering, as has artificial intelligence design based on the deep neural network technique [45]. In studies using image processing algorithms, the detection

of faulty versus error free products passing by on a conveyor belt was achieved using median and Canny edge detection filters [46]. The equation model for the median filter is given in Equation 1.

$$I'(u, v) \leftarrow \text{median}\{I(u + i, v + j) | (i, j) \in R\} \quad (1)$$

Using the Prewitt approach, the edges in brain CTA images are determined at points of maximum gradient. Edges are located by approximating the size of the image gradient. The horizontal and vertical kernels of the Prewitt algorithm are designated Px and Py, respectively. The input matrix is convolved with the Prewitt kernel (Px, Py) and the resulting gradient component represents the output.

$$\begin{bmatrix} -1 & 0 & 1 \\ -1 & 0 & 1 \\ -1 & 0 & 1 \end{bmatrix} \quad \begin{bmatrix} -1 & -1 & -1 \\ 0 & 0 & 0 \\ 1 & 1 & 1 \end{bmatrix} \quad (2)$$

The Prewitt method is a computationally simple process that produces noisier results than classical edge detection algorithms [47].

Smoothing is a filtering process used to reduce noise in datasets and constitutes an essential technique frequently employed in image processing applications. The new image obtained following the smoothing process is rendered suitable for edge removal. In the present study, the main objective was to perform edge extraction utilizing the Sobel, Prewitt, and Canny filters at the points where the slope is softened.

The Sobel method, like the Canny and Prewitt algorithms, is a classical filtering technique utilized in edge detection. This widely used filter yields frequencies of high range differences discerned in the gray levels of images [48]. Gradients are obtained by processing neighboring pixels; matrices of different sizes, called “edge detection operator” and “kernel matrix”, are used in this process. In noisy images, edges contain high frequencies, and reducing noise may distort and/or blur edges, thus rendering edge detection in such cases difficult [49]. The Sobel method has been applied to improve edge detection in brain tumor MR images; the proposed algorithm was determined to be the most optimal technique [47].

Sobel convolution matrices (Sx, Sy) were manipulated to perform scanning on the brain CTA images used in this study, thus yielding gradient information on the x and y coordinates.

$$\begin{bmatrix} -1 & 0 & 1 \\ -2 & 0 & 2 \\ -1 & 0 & 1 \end{bmatrix} \quad \begin{bmatrix} -1 & -2 & -1 \\ 0 & 0 & 0 \\ 1 & 2 & 1 \end{bmatrix} \quad (3)$$

Figure 2 shows a sample image of a brain with an aneurysm and the images obtained using Canny, Median, Prewitt, Smoothing and Sobel filters, respectively.

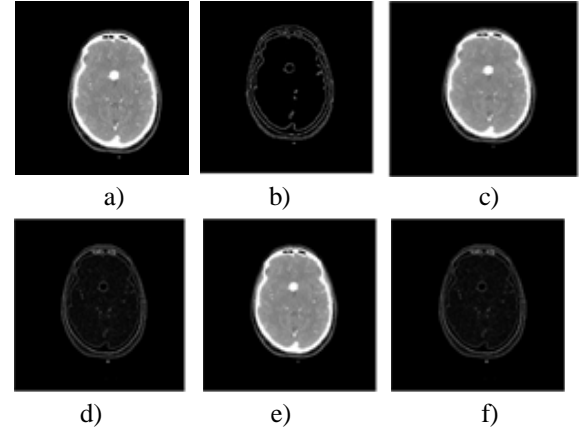


Figure 2. Filtered images of aneurysm a) Raw b) Canny c) Median d) Prewitt e) Smoothing f) Sobel

Canny, Prewitt, and Sobel are effective filters for edge detection. The filtered images obtained by applying these filters to CTA scans were subsequently used as inputs for the CNN models. In this context, images processed with the Prewitt, Sobel, and Canny filters, respectively, achieved high accuracy rates in aneurysm classification. When compared to raw images, it was observed that Prewitt filtered images demonstrated superior classification performance. In addition, the median and smoothing filters, which were employed to reduce noise, were compared. In this analysis, aneurysms were successfully classified with an accuracy of 99.72% for images processed with the smoothing filter and 99.45% for those processed with the median filter.

APPLIED CNN

In this architecture, the input data consisted of images [50]. The brain CTA images used in CNN underwent different image analyses, classified as axial, sagittal, and coronal sections. For the present study, brain CTA coronal images were selected as the input to be used in CNN. Coronal images have become the input of choice because they contain more sensitive images. The deep features of brain CTA images used to identify patients with cerebral aneurysms were extracted using DL networks. Among the DL based CNN architectures, AlexNet, DenseNet201, GoogLeNet, InceptionResNetV2, Inceptionv3, MobileNetv2, NASNetMobile, ResNet18, ResNet50, ResNet101, ShuffleNet, SqueezeNet, VGG16, VGG19, Xception networks were used in the current study.

Five different datasets, both raw and filtered, consisting of brain CTA images were applied as input images to deep neural networks. The training accuracy and performance metrics of the CNNs were then evaluated. By comparing both CNNs and the various datasets used as input images, aneurysm detection was achieved with the highest level of accuracy known in the literature.

The image data underwent preprocessing and were prepared for input into the network, where predictions were generated on the trained network. Transfer learning is optimal for applying a DL model when the number of input images is insufficient. In the implementation of the

transfer learning strategy, the dataset was first imported and prepared for analysis. Subsequently, 15 different pretrained CNN architectures were selected and applied sequentially. For model training, 70% of the data was allocated for training and 30% for validation. The models were trained using transfer learning, and the training progress, including accuracy metrics, was monitored and evaluated through exported training progress graphs. Network training requires a high performance GPU or CPU. For processing the CTA image data, the MATLAB program was used on a system equipped with 16 GB of RAM, an Intel Core i7 processor, and an NVIDIA

GeForce RTX 3070 GPU. The image data were randomly divided, with 70% allocated for training and 30% for validation. The following parameters were selected for Momentum Stochastic Gradient Descent (SGDM) optimization in training: learning rate 1e-3, validation frequency 30, maximum epoch 64, and a minimum batch size of 50. were selected using optimization in training. Following the training, the input images were categorized into two class output, aneurysmal and non aneurysmal. The steps followed in the study are shown in Figure 3.

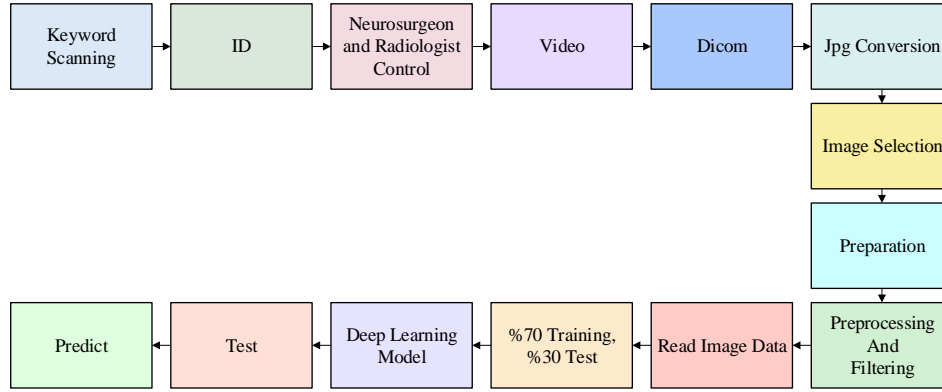


Figure 3. Recommended methodology for applied DL models

EXPERIMENTAL RESULTS

Performance metrics for DL models are presented in this section. We calculated 80 results for 15 different CNNs implemented with 6 different datasets. These 80 results calculated for these datasets are presented. We used MATLAB programming in the implementation of this proposed filtering based DL architecture.

Performance evaluation metric

Confusion matrix components are used as criteria to determine the performance metrics of the system. These components are identified as Accuracy (ACC), Sensitivity (SEN), Specificity (SPE), Precision (PRC), and F-Score. The accuracy metric summarizes the proportion of all correctly classified instances, combining both true positives and true negatives. Sensitivity (or recall) specifically emphasizes the model's strength in detecting positive cases. In contrast, specificity reflects the model's efficiency in correctly recognizing negative cases, thereby reducing false positives. Precision captures the proportion of true positives among all predicted positives. The F-score integrates precision and sensitivity into a single metric, providing a balanced evaluation particularly when the data distribution between classes is uneven. For performance evaluations, calculations are made by substituting the coefficients in the confusion matrices into the equation models for each component. Comparative analyses were thus carried out for each of the CNNs employed.

Accuracy;

$$ACC = \frac{tp + tn}{tp + tn + fp + fn} \quad (4)$$

Sensitivity;

$$SEN_{aneurysm} = \frac{tp}{tp + fn} \quad SEN_{non-aneurysm} = \frac{tn}{tn + fp} \quad (5)$$

Specificity;

$$SPE_{aneurysm} = \frac{tn}{tn + fp} \quad SPE_{non-aneurysm} = \frac{tp}{tp + fn} \quad (6)$$

Precision;

$$PRC_{aneurysm} = \frac{tp}{tp + fp} \quad PRC_{non-aneurysm} = \frac{tn}{tn + fn} \quad (7)$$

F-Score;

$$F - score_{aneurysm} = \frac{2xtp}{2xtp + fp + fn} \quad (8)$$

$$F - score_{non-aneurysm} = \frac{2xtn}{2xtn + fp + fn} \quad (9)$$

Confusion matrices of the learning conducted using brain CTA images resulting from the application of different filtering techniques are presented in Figure 4. Performance metrics were calculated by taking into account the components of these matrices. The fundamental components used to evaluate model performance are as follows: true positives (tp) represent cases where the model correctly predicts a positive instance, while true negatives (tn) indicate correct identification of negative instances. false positives (fp) occur when the model incorrectly classifies a negative instance as positive, and false negatives (fn) refer to

positive instances that are incorrectly classified as negative. These metrics are essential for comprehensively assessing the accuracy and reliability of the model. The darker green color indicates the number of tn, while the amount of tp is shown in light green. Similarly, the dark pink color signifies the number of fp whereas light pink indicates the amount of fn. According to our findings, the networks yielding the best performance metric values for the raw image dataset and the datasets whose images were filtered using the Canny, median, Prewitt, smoothing, and Sobel methods were AlexNet, AlexNet, AlexNet, ResNet50, VGG19, and ResNet101, respectively.

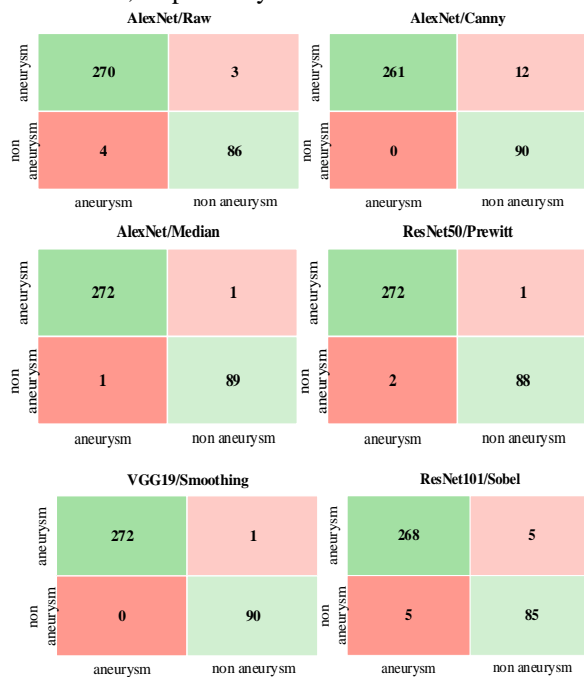


Figure 4. Confusion matrices

For the AlexNet deep neural network with the highest prediction accuracy in the raw image dataset, 270 tn, 3 fn and 4 fp, 86 tp are the outputs of the network's testing process. For the AlexNet deep neural network on Canny filtered images, 261 tn, 12 fn and 0 fp, 90 tp are the outputs of the test process of the network. In the median filtered images, 272 tn, 1 fn and 1 fp, 89 tp for the AlexNet deep neural network are the outputs of the test process of the network. For the ResNet50 deep neural network in Prewitt filtered images, 272 tn, 1 fn and 2 fp, 88 tp are the outputs of the network testing process. For the VGG19 deep neural network in smoothing filtered images, 272 tn, 1 fn and 0 fp, 90 tp are the outputs of the network testing process. For the ResNet101 deep neural network in Sobel filtered images, 268 tn, 5 fn and 5 fp, 85 tp are the outputs of the test process of the network.

The classification performance of the proposed model was assessed by plotting the Receiver Operating Characteristic (ROC) curve, as presented in Figure 5.

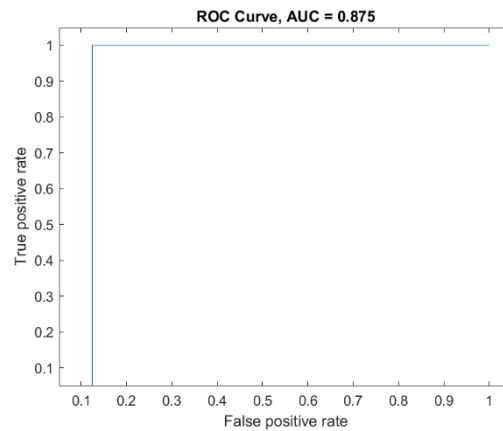


Figure 5. ROC Curve

The ROC curve provides a comprehensive evaluation of the model's ability to distinguish between healthy and diseased cases across various threshold values. The Area Under the Curve (AUC) was found to be 0.875, which indicates a strong discriminative capability. These results demonstrate that the model is effective in differentiating between the two classes and may be considered a promising tool for clinical decision support. Notably, these findings were obtained using the VGG19 network trained on a dataset preprocessed with a smoothing filter.

Filtering based results

In this study, the following parameter settings were used for image filtering: The Canny edge detector was applied with threshold values of [0 0.35]; the median filter used a 3×3 window; both Prewitt and Sobel filters were implemented with standard 3×3 kernels using MATLAB's default settings; and bilateral smoothing was performed with a degree of smoothing (DoS) parameter set to 1000. All parameter choices were based on preliminary experiments to ensure optimal performance for the dataset.

A dataset consisting of filtered brain CTA images for 200 patients was applied to 15 CNNs as input layers. A total of 1211 CTA images in this set with an image size of 512x512x3 were used in training the networks. The image sizes applied to the input layers were different for each network; information on training accuracy and time is given in Tables 2 and 3. Of the images, 70% were randomly allocated for training and 30% for validation. Regarding training, the maximum epochs chosen were 6, 32, and 64, minimum batch sizes were 10 and 50, and the initial learning rate was 0.0001 using SGDM optimization.

Table 2. Accuracies of CNNs applying different data sets

Network	Raw (%)	Canny (%)	Median (%)	Prewitt (%)	Smoothing (%)	Sobel (%)
AlexNet	98.07	96.69	99.45	98.90	98.07	94.21
DenseNet201	97.52	92.29	98.35	98.90	98.62	95.04
GoogLeNet	92.84	84.3	86.5	91.18	98.62	89.26
InceptionResNetV2	88.15	84.3	83.2	97.80	96.97	81.82
Inceptionv3	94.4	92.56	90.63	96.42	96.42	85.67
MobileNetv2	92.84	90.08	89.26	97.52	99.17	86.78
NASNetMobile	87.05	84.02	82.64	92.01	93.11	91.46
ResNet18	94.77	94.49	92.56	96.69	97.80	91.46
ResNet50	96.69	95.32	96.14	99.17	98.07	94.21
ResNet101	95.59	92.84	98.35	98.35	95.59	97.25
ShuffleNet	92.84	91.74	95.04	97.80	99.17	84.85
SqueezeNet	87.33	85.12	87.05	93.39	90.91	88.15
VGG16	92.84	88.42	89.26	96.14	97.52	87.05
VGG19	90.08	93.66	84.85	98.90	99.72	91.18
Xception	88.71	83.20	77.96	90.08	88.98	80.72

In training using raw images, the highest accuracy shown in Table 3 is 98.07%, attained by the AlexNet network. According to the training accuracy results for Canny filtered images, this same deep neural network yielded the best result among the applied CNNs, with an accuracy value of 96.69%. AlexNet also performed the best for median filtered images, achieving an accuracy of

99.45%. The ResNet50 deep neural network was deemed most suitable for Prewitt filtered images, with 99.17% accuracy. The VGG19 network yielded the highest accuracy, at 99.72%, for smoothing filtered images, while the ResNet101 network performed best for Sobel filtered images, with an accuracy of 97.25%.

Table 3. Training times of CNNs on filtered images (sec)

Network	Raw	Canny	Median	Prewitt	Smoothing	Sobel
AlexNet	930	330	201	198	186	162
DenseNet201	736	802	771	2865	2441	412
GoogLeNet	116	69	107	337	520	158
InceptionResNetV2	541	774	1695	1501	1343	1995
Inceptionv3	209	202	300	807	1022	371
MobileNetv2	159	203	257	335	557	105
NASNetMobile	261	1314	373	643	1095	2318
ResNet18	49	142	114	260	147	93
ResNet50	140	148	287	671	464	115
ResNet101	190	189	469	1531	849	435
ShuffleNet	103	144	256	169	305	161
SqueezeNet	43	136	112	264	214	62
VGG16	98	115	133	1019	808	94
VGG19	236	232	222	1147	1200	205

Xception	163	432	375	18004	7630	419
----------	-----	-----	-----	-------	------	-----

Training times for CNNs in which raw and filtered brain CTA images were applied as input images are presented in Table 4. The calculated training times corresponding to the highest values for accuracy were as follows:

- 930 seconds for the raw dataset,
 - 330 seconds for the Canny filtered dataset,
 - 201 seconds for the median filtered dataset,
 - 671 seconds for the Prewitt filtered dataset,
 - 1200 seconds for the smoothing filtered dataset,
- 435 seconds for the Sobel filtered dataset.

Table 4 summarizes the architectural properties of the deep neural networks evaluated in this study, including the number of layers, layer depth, and input image size for each model.

Table 4. CNN Model Architecture and Hyperparameters

Network	Number of Layers	Layer Depth	Input Image Size
AlexNet	25	8	227x227x3
DenseNet201	709	201	224x224x3
GoogLeNet	144	22	224x224x3
InceptionResNetV2	825	164	299x299x3
Inceptionv3	316	48	299x299x3
MobileNetv2	155	53	224x224x3
NASNetMobile	*	*	224x224x3
ResNet18	72	18	224x224x3
ResNet50	177	50	224x224x3
ResNet101	347	101	224x224x3
ShuffleNet	300	50	224x224x3
SqueezeNet	68	18	227x227x3
VGG16	41	16	224x224x3
VGG19	47	19	224x224x3
Xception	71	71	299x299x3

Note: *The NASNet Mobile neural network does not consist of a linear sequence of modules.

These parameters are essential for understanding the computational complexity and feature extraction capabilities of the networks. It should be noted that the NASNet Mobile architecture does not follow a linear sequence of modules; therefore, its layer count and depth are not directly comparable to the other models. This comparative overview provides important context for interpreting the subsequent performance analyses.

DISCUSSION

In order to make predictions with high accuracy through transfer learning, the brain CTA image data were preprocessed and prepared to be applied as CNN inputs. Following the training, the input images were categorized as output images in two classes: those with and those without aneurysms.

Among the CNNs applied to raw images, AlexNet exhibited the best performance metric with an accuracy of 98.07%. Accuracy and loss graphs pertaining to the training process are shown in Figure 6.

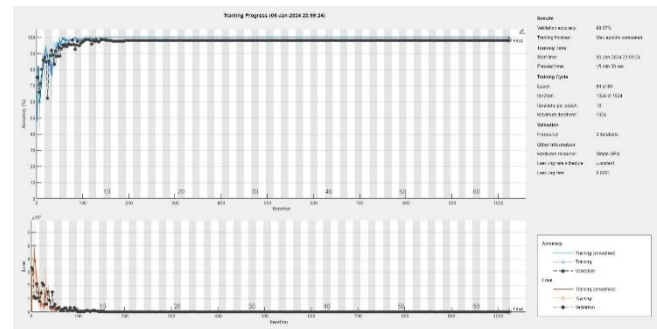


Figure 6. AlexNet training graph applied to raw images

AlexNet also performed best in terms of accuracy for Canny filtered images, with a value of 96.69%. For median filtered images, AlexNet also had the best performance metric with respect to accuracy, at 99.45%. Of the CNNs applied to Prewitt filtered images, the best performance metric was generated by ResNet50, with an accuracy of 99.17%. Among the CNNs applied to Sobel filtered images, ResNet101 had the best performance metric with a 97.25% accuracy rate.

For smoothing filtered images, VGG19 exhibited the best performance metric, with 99.72% accuracy. Figure 7 shows the accuracy and loss graphs of the training process of the VGG19 network for the highest accuracy on filtered datasets.

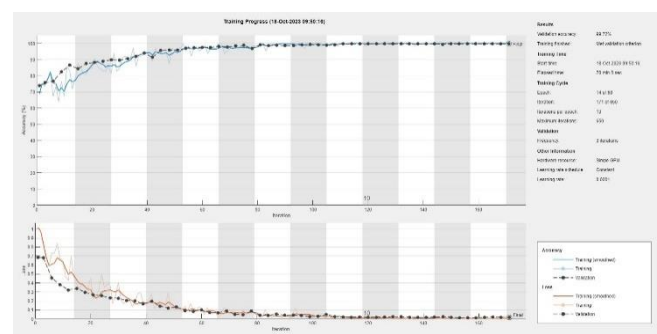


Figure 7. VGG19 training graph applied to smoothing filtered images

Comparative results

In this study, various filtering methods were applied to improve the quality of brain CTA images for cerebral aneurysm detection. Canny edge detection was chosen due to its high accuracy in edge identification and robustness to noise; however, it is computationally intensive and may require parameter optimization. Median filtering was used to suppress image noise while preserving essential structural details, although excessive application can result in the blurring of fine features. The

Prewitt filter was selected for its simplicity and computational efficiency in estimating image intensity gradients, but it is more sensitive to noise and less precise in edge localization. Smoothing filters were employed to further reduce noise and enhance the suitability of images for subsequent processing, yet they may also blur important structural details and edges. Lastly, the Sobel filter, while straightforward and effective for edge detection, is susceptible to edge blurring and is less robust to noise compared to more advanced techniques. The selection and implementation of these filters were carefully considered to optimize image quality and enhance the performance of DL models in cerebral aneurysm detection.

The performance metrics presented in Table 4 belong to CNNs with the highest training accuracy, where raw datasets and those undergoing five different filtering

methods were used as input images. In addition to the classification of raw images according to these criteria, training was completed for 15 different CNNs by preparing datasets to which preprocessing and necessary filtering methods were applied. When evaluating with the parameter of accuracy as the determining criterion, the highest rate was obtained with smoothing, followed by the median and Prewitt filtered datasets. Unlike the literature, in the present study, not only were raw images assessed, but comparisons were also performed using filtered datasets. The results obtained indicate that preprocessing and filtering methods for aneurysm detection play an important role in increasing training accuracy.

Table 5. Network performance metrics with the highest accuracy in image datasets

Type of Image	Class	Sens.	Spec.	Prec.	F-Sc.	Acc.
Raw	Aneurysm	0.9890	0.9555	0.9854	0.9872	0.9807
	Non aneurysm	0.9555	0.9890	0.9662	0.9608	
Canny Filter	Aneurysm	0.9560	1	1	0.9775	0.9669
	Non aneurysm	1	0.9560	0.8823	0.9375	
Median Filter	Aneurysm	0.9963	0.9888	0.9963	0.9963	0.9944
	Non aneurysm	0.9888	0.9963	0.9888	0.9888	
Prewitt Filter	Aneurysm	0.9963	0.9777	0.9927	0.9945	0.9917
	Non aneurysm	0.9777	0.9963	0.9887	0.9832	
Smoothing Filter	Aneurysm	0.9963	1	1	0.9981	0.9972
	Non aneurysm	1	0.9963	0.9890	0.9944	
Sobel Filter	Aneurysm	0.9816	0.9444	0.9816	0.9816	0.9724
	Non aneurysm	0.9444	0.9816	0.9444	0.9444	

The high accuracy and sensitivity achieved in this study highlight the combined impact of advanced image processing techniques and DL algorithms in the detection of cerebral aneurysms. By integrating effective image preprocessing methods with state of the art DL architectures, our approach demonstrates clinically relevant performance that can support radiologists in routine practice. This combination not only automates the initial screening process reducing the workload of radiologists and enabling them to focus on more complex cases but also enhances the detection of small aneurysms, which is essential for early diagnosis and timely intervention. These results indicate that the proposed method has the potential to improve patient outcomes by enabling earlier and more accurate detection of cerebral aneurysms.

The use of a novel, real world dataset and the application of advanced image processing techniques to CTA images have enabled our model to achieve the highest reported accuracy in aneurysm detection. This high level of diagnostic performance has the potential to significantly reduce interpretation errors by radiologists, thereby improving the reliability of aneurysm identification in clinical practice. Moreover, the automated and accurate detection provided by the proposed approach can serve as a valuable decision support tool for neurosurgeons, aiding in the planning of appropriate treatment strategies

for patients with aneurysms. Ultimately, these advancements may contribute to more timely and effective patient management, leading to improved clinical outcomes.

One of the primary limitations of this study is the relatively small sample size and the use of data from a single center, which may affect the generalizability of the findings. In future research, increasing the number of patient samples and incorporating data from multiple institutions are planned to enhance the robustness and external validity of the proposed approach. Additionally, including aneurysm images from patients in different geographic regions could provide a more comprehensive evaluation of the model's performance across diverse populations. Finally, future studies may also compare DL models using images obtained from various diagnostic modalities, further broadening the clinical applicability of the developed methods.

CONCLUSION

DL applications have been widely used following advances in technology to diagnose aneurysms in CTA images. In the present study, CTA images were obtained depicting the brains of patients both with and without cerebral aneurysms. Filter methods were then applied to our dataset of brain CTA images. The novel images thus created were used in 15 different CNN inputs to scan for

aneurysms. The results showed that the dataset enhanced with the smoothing filter yielded the highest known performance, achieving 99.72% accuracy. Using a new dataset that is not yet available in the literature, the training achieved a high rate of validation with 99.63% sensitivity, 100% specificity, 100% precision, and an f-score of 99.81%. Evaluation of the images resulted in the detection of 272 true negatives, 1 false negative, and 90 true positives for patients with aneurysms, and 0 false positives for patients without aneurysms.

Contributions of the present study include:

A dataset comprised of current and previously unused actual images was employed, thus adding a novel dataset to the literature.

In addition to the raw images, the performance metrics of deep neural networks were compared using five different filtering methods, with the results showing that preprocessing and filtering methods increased the training accuracy in aneurysm detection.

The study highlights the superiority of artificial intelligence based DL models in aneurysm detection. Future studies may increase the sample size and incorporate datasets from multiple institutions to enhance the generalizability of the results. In addition, different filter methods can be applied to angiography images. DL models can be compared using images obtained using various diagnostic methods. This method of comparison, which provides high accuracy in disease detection, can also be employed to classify different diseases.

Author contribution statements

All authors contributed to the study's conceptualization, investigation, writing – review & editing, software, methodology, validation, formal analysis, writing – original draft, visualization, data curation, supervision, project administration, resources. All authors read and approved the final manuscript.

Ethics committee approval and conflict of interest statement

This research was approved on ethical grounds by the Non-Interventional Research Ethics Committee, Firat University Ethics Board, on 17 September 2020 (2020/12–04).

“There is no conflict of interest with any person/institution in the article prepared”.

REFERENCES

[1] Kaya V. Anterior Kommunikan Arter Ve Anterior Kommunikan Arter İle İlişkili Anterior Sistem Anevrizmalarında “Morfolojik Ve Hemodinamik Faktörlerin” Anevrizma Ruptürü İle İlişkisi. İnönü, 2018.

[2] Lawton MT, Vates GE. Subarachnoid Hemorrhage. *N Engl J Med* 2017;377:257–66. <https://doi.org/10.1056/NEJMcpl605827>.

[3] Jin H, Yin Y, Hu M, Yang G, Qin L. Fully automated unruptured intracranial aneurysm detection and segmentation from digital subtraction angiography series using an end-to-end spatiotemporal deep

neural network, 2019. <https://doi.org/10.1117/12.2512623>.

[4] Dai X, Huang L, Qian Y, Xia S, Chong W, Liu J, et al. Deep learning for automated cerebral aneurysm detection on computed tomography images. *Int J Comput Assist Radiol Surg* 2020. <https://doi.org/10.1007/s11548-020-02121-2>.

[5] Gu F, Wu X, Wu W, Wang Z, Yang X, Chen Z, et al. Performance of deep learning in the detection of intracranial aneurysm: A systematic review and meta-analysis. *Eur J Radiol* 2022;155:110457. <https://doi.org/10.1016/j.ejrad.2022.110457>.

[6] Heit JJ, Honce JM, Yedavalli VS, Baccin CE, Tatit RT, Copeland K, et al. RAPID Aneurysm: Artificial intelligence for unruptured cerebral aneurysm detection on CT angiography. *J Stroke Cerebrovasc Dis* 2022;31:106690. <https://doi.org/10.1016/j.jstrokecerebrovasdis.2022.106690>.

[7] Buchlak QD, Milne MR, Seah J, Johnson A, Samarasinghe G, Hachey B, et al. Charting the potential of brain computed tomography deep learning systems. *J Clin Neurosci* 2022. <https://doi.org/10.1016/j.jocn.2022.03.014>.

[8] Wei X, Jiang J, Cao W, Yu H, Deng H, Chen J, et al. Artificial intelligence assistance improves the accuracy and efficiency of intracranial aneurysm detection with CT angiography. *Eur J Radiol* 2022;149:110169. <https://doi.org/10.1016/j.ejrad.2022.110169>.

[9] Wang J, Ti L, Sun X, Yang R, Zhang N, Sun K. DSA Image Analysis of Clinical Features and Nursing Care of Cerebral Aneurysm Patients Based on the Deep Learning Algorithm. *Scanning* 2022;2022:1–6. <https://doi.org/10.1155/2022/8485651>.

[10] Tasci B, Tasci I. Deep feature extraction based brain image classification model using preprocessed images: PDRNet. *Biomed Signal Process Control* 2022;78:103948. <https://doi.org/10.1016/j.bspc.2022.103948>.

[11] Lehnen NC, Haase R, Schmeel FC, Vatter H, Dorn F, Radbruch A, et al. Automated Detection of Cerebral Aneurysms on TOF-MRA Using a Deep Learning Approach: An External Validation Study. *Am J Neuroradiol* 2022;43:1700–5. <https://doi.org/10.3174/ajnr.A7695>.

[12] Shi Z, Miao C, Schoepf UJ, Savage RH, Dargis DM, Pan C, et al. A clinically applicable deep-learning model for detecting intracranial aneurysm in computed tomography angiography images. *Nat Commun* 2020;11:6090. <https://doi.org/10.1038/s41467-020-19527-w>.

[13] Terasaki Y, Yokota H, Tashiro K, Maejima T, Takeuchi T, Kurosawa R, et al. Multidimensional Deep Learning Reduces False-Positives in the Automated Detection of Cerebral Aneurysms on Time-Of-Flight Magnetic Resonance Angiography: A Multi-Center Study. *Front Neurol* 2022;12. <https://doi.org/10.3389/fneur.2021.742126>.

- [14] Chen G, Meng C, Ruoyu D, Dongdong W, Liqin Y, Wei X, et al. An automatic detection method of cerebral aneurysms in time-of-flight magnetic resonance angiography images based on attention 3D U-Net. *Comput Methods Programs Biomed* 2022;225:106998. <https://doi.org/10.1016/j.cmpb.2022.106998>.
- [15] Chen G, Yifang B, Jiajun Z, Dongdong W, Zhiyong Z, Ruoyu D, et al. Automated unruptured cerebral aneurysms detection in TOF MR angiography images using dual-channel SE-3D UNet: a multi-center research. *Eur Radiol* 2023. <https://doi.org/10.1007/s00330-022-09385-z>.
- [16] Stember JN, Chang P, Stember DM, Liu M, Grinband J, Filippi CG, et al. Convolutional Neural Networks for the Detection and Measurement of Cerebral Aneurysms on Magnetic Resonance Angiography. *J Digit Imaging* 2019;32:808–15. <https://doi.org/10.1007/s10278-018-0162-z>.
- [17] Di Noto T, Marie G, Tourbier S, Alemán-Gómez Y, Saliou G, Bach Cuadra M, et al. An Anatomically-Informed 3D CNN for Brain Aneurysm Classification with Weak Labels, 2020, p. 56–66. https://doi.org/10.1007/978-3-030-66843-3_6.
- [18] Tasci B. Automated ischemic acute infarction detection using pre-trained CNN models' deep features. *Biomed Signal Process Control* 2023;82:104603. <https://doi.org/10.1016/j.bspc.2023.104603>.
- [19] Nakao T, Hanaoka S, Nomura Y, Sato I, Nemoto M, Miki S, et al. Deep neural network-based computer-assisted detection of cerebral aneurysms in MR angiography. *J Magn Reson Imaging* 2018;47:948–53. <https://doi.org/10.1002/jmri.25842>.
- [20] Heit JJ, Honce JM, Yedavalli VS, Baccin CE, Tatit RT, Copeland K, et al. RAPID Aneurysm: Artificial intelligence for unruptured cerebral aneurysm detection on CT angiography. *J Stroke Cerebrovasc Dis* 2022. <https://doi.org/10.1016/j.jstrokecerebrovasdis.2022.106690>.
- [21] Suwalska A, Siuda J, Kocot S, Zmuda W, Rudzinska-Bar M, Polanska J. Activation maps of convolutional neural networks as a tool for brain degeneration tracking in early diagnosis of dementia in Parkinson's disease based on magnetic resonance imaging. *Signal, Image Video Process* 2023;17:4115–21. <https://doi.org/10.1007/s11760-023-02643-7>.
- [22] Kutan F, Aynur Ö. Gürültü Filtreleme Uygulamalarının Medikal Görüntüler Üzerindeki Performanslarının Değerlendirilmesi. *Eur J Sci Technol* 2020;265–71. <https://doi.org/10.31590/ejosat.779957>.
- [23] Meng C, Yang D, Chen D. Cerebral aneurysm image segmentation based on multi-modal convolutional neural network. *Comput Methods Programs Biomed* 2021;208:106285. <https://doi.org/10.1016/j.cmpb.2021.106285>.
- [24] Öziç MÜ, Özşen S. Üç Boyutlu T1 Ağırlıklı Manyetik Rezonans Görüntülerinde Ön İşleme Yöntemleri. *Eur J Sci Technol* 2020;227–40. <https://doi.org/10.31590/ejosat.719062>.
- [25] Shi Z, Miao C, Schoepf UJ, Savage RH, Dargis DM, Pan C, et al. A clinically applicable deep-learning model for detecting intracranial aneurysm in computed tomography angiography images. *Nat Commun* 2020. <https://doi.org/10.1038/s41467-020-19527-w>.
- [26] Qiu J, Tan G, Lin Y, Guan J, Dai Z, Wang F, et al. Automated detection of intracranial artery stenosis and occlusion in magnetic resonance angiography: A preliminary study based on deep learning. *Magn Reson Imaging* 2022;94:105–11. <https://doi.org/10.1016/j.mri.2022.09.006>.
- [27] Liao J, Liu L, Duan H, Huang Y, Zhou L, Chen L, et al. Using a Convolutional Neural Network and Convolutional Long Short-term Memory to Automatically Detect Aneurysms on 2D Digital Subtraction Angiography Images: Framework Development and Validation. *JMIR Med Informatics* 2022;10:e28880. <https://doi.org/10.2196/28880>.
- [28] Vidhya SRS, Arunachalam AR. Automated Detection of False positives and false negatives in Cerebral Aneurysms from MR Angiography Images by Deep Learning Methods. 2021 Int. Conf. Syst. Comput. Autom. Netw., IEEE; 2021, p. 1–4. <https://doi.org/10.1109/ICSCAN53069.2021.9526520>.
- [29] Lei X, Yang Y. Deep Learning-Based Magnetic Resonance Imaging in Diagnosis and Treatment of Intracranial Aneurysm. *Comput Math Methods Med* 2022. <https://doi.org/10.1155/2022/1683475>.
- [30] Su R, van der Sluijs M, Cornelissen SAP, Lycklama G, Hofmeijer J, Majoie CBLM, et al. Spatio-temporal deep learning for automatic detection of intracranial vessel perforation in digital subtraction angiography during endovascular thrombectomy. *Med Image Anal* 2022. <https://doi.org/10.1016/j.media.2022.102377>.
- [31] Mei Y jia, Hu R ting, Lin J, Xu H yu, Wu L ya, Li H peng, et al. Diagnosis of Middle Cerebral Artery Stenosis Using Transcranial Doppler Images Based on Convolutional Neural Network. *World Neurosurg* 2022. <https://doi.org/10.1016/j.wneu.2022.01.068>.
- [32] Dai X, Huang L, Qian Y, Xia S, Chong W, Liu J, et al. Deep learning for automated cerebral aneurysm detection on computed tomography images. *Int J Comput Assist Radiol Surg* 2020;15:715–23. <https://doi.org/10.1007/s11548-020-02121-2>.
- [33] Ueda D, Yamamoto A, Nishimori M, Shimono T, Doishita S, Shimazaki A, et al. Deep learning for MR angiography: Automated detection of cerebral aneurysms. *Radiology* 2019. <https://doi.org/10.1148/radiol.2018180901>.
- [34] Rahman AI, Bhuiyan S, Reza ZH, Zaheen J, Khan TAN, Karim DZ. Intracranial Hemorrhage

- Detection on CT Scan Images using Transfer Learning Approach of Convolutional Neural Network. *ACM Int. Conf. Proceeding Ser.*, 2022. <https://doi.org/10.1145/3542954.3542980>.
- [35] Ou C, Qian Y, Chong W, Hou X, Zhang M, Zhang X, et al. A deep learning-based automatic system for intracranial aneurysms diagnosis on three-dimensional digital subtraction angiographic images. *Med Phys* 2022. <https://doi.org/10.1002/mp.15846>.
- [36] Ivantsits M, Goubergrits L, Kuhnigk JM, Huellebrand M, Bruening J, Kossen T, et al. Detection and analysis of cerebral aneurysms based on X-ray rotational angiography - the CADA 2020 challenge. *Med Image Anal* 2022. <https://doi.org/10.1016/j.media.2021.102333>.
- [37] Sathish Kumar L, Hariharasitaraman S, Narayanasamy K, Thinakaran K, Mahalakshmi J, Pandimurugan V. AlexNet approach for early stage Alzheimer's disease detection from MRI brain images. *Mater. Today Proc.*, 2021. <https://doi.org/10.1016/j.matpr.2021.04.415>.
- [38] Di Noto T, Marie G, Tourbier S, Alemán-Gómez Y, Esteban O, Saliou G, et al. Towards Automated Brain Aneurysm Detection in TOF-MRA: Open Data, Weak Labels, and Anatomical Knowledge. *Neuroinformatics* 2022. <https://doi.org/10.1007/s12021-022-09597-0>.
- [39] Guzmán Ortiz S, Hurtado Ortiz R, Jara Gavilanes A, Ávila Faican R, Parra Zambrano B. A serial image analysis architecture with positron emission tomography using machine learning combined for the detection of lung cancer. *Rev Española Med Nucl e Imagen Mol (English Ed)* 2024;43:500003. <https://doi.org/10.1016/j.remnie.2024.500003>.
- [40] Özmen T, Kuzu Ü, Koçyiğit Y, Sarnel H. Early stage diabetes prediction by features selection with metaheuristic methods. *Pamukkale Univ J Eng Sci* 2023;29:596–606. <https://doi.org/10.5505/pajes.2022.82610>.
- [41] Karahan T, Nabiye V. Plant identification with convolutional neural networks and transfer learning. *Pamukkale Univ J Eng Sci* 2021;27:638–45. <https://doi.org/10.5505/pajes.2020.84042>.
- [42] Alakuş TB, Türkoğlu İ. Prediction of human protein functions with protein mapping techniques and deep learning model. *Pamukkale Univ J Eng Sci* 2022;28:255–65. <https://doi.org/10.5505/pajes.2021.51261>.
- [43] Sez E, Üncü Ya, Yardımcı A. Prematüre Retina Kan Damarlarının Tespitinde Farklı Görüntü İşleme Yöntemlerinin Performanslarının Karşılaştırılması. *Süleyman Demirel Üniversitesi Fen Edeb Fakültesi Fen Derg* 2023;18:62–75. <https://doi.org/10.29233/sdufeffd.1220516>.
- [44] Wu F, Zhu C, Xu J, Bhatt MW, Sharma A. Research on image text recognition based on canny edge detection algorithm and k-means algorithm. *Int J Syst Assur Eng Manag* 2022;13:72–80. <https://doi.org/10.1007/s13198-021-01262-0>.
- [45] Gupta IK, Choubey A, Choubey S. Artificial intelligence with optimal deep learning enabled automated retinal fundus image classification model. *Expert Syst* 2022;39. <https://doi.org/10.1111/exsy.13028>.
- [46] Uzun Y, Boyacıgil M. Raspberry PI Tabanlı Görüntü İşleme Uygulaması Geliştirilmesi. *Osmaniye Korkut Ata Üniversitesi Fen Bilim Enstitüsü Derg* 2023;6(2):1067–78.
- [47] A S RA, Gopalan S. Comparative Analysis of Eight Direction Sobel Edge Detection Algorithm for Brain Tumor MRI Images. *Procedia Comput Sci* 2022;201:487–94. <https://doi.org/10.1016/j.procs.2022.03.063>.
- [48] Padlia M, Sharma J. Fractional Sobel Filter Based Brain Tumor Detection and Segmentation Using Statistical Features and SVM, 2019, p. 161–75. https://doi.org/10.1007/978-981-13-0776-8_15.
- [49] Bilal Macit H, Koyun A. An Active Image Forgery Detection Approach Based on Edge Detection. *Comput Mater Contin* 2023;75:1603–19. <https://doi.org/10.32604/cmc.2023.036216>.
- [50] Gurkan C, Kozalioglu S, Palandoken M. Real Time Mask Detection, Social Distance and Crowd Analysis using Convolutional Neural Networks and YOLO Architecture Designs. *Acad Perspect Procedia* 2021;4:195–204. <https://doi.org/10.33793/acperpro.04.01.29>.